*Larhyss Journal, ISSN 1112-3680, n°54, Jun 2023, pp.217-237*


# VELOCITY DISTRIBUTION IN A CONTROLLED HYDRAULIC JUMP IN A COMPOUND CHANNEL: AN EXPERIMENTAL AND MACHINE LEARNING (ML) STUDY

***BOURICHE F.[1]*, DEBABECHE M.[1], CARVALHO RITA F.[2], DJEDDOU M.[3]***

[1] Research Laboratory in Civil and Hydraulic Engineering, Sustainable Development and Environment LARGHYD), University of Biskra, Algeria
[2] Department of Civil Engineering, Faculty of Sciences and Technology, University of Coimbra, MARE – Marine and Environmental Sciences Centre, ARNET - Aquatic Research Network, Coimbra, Portugal
[3] Research Laboratory in Subterranean and Surface Hydraulics, (LARHYSS) University of Biskra, Algeria

*(*) fouzi.bouriche@univ-biskra.dz*

Research Article – Available at http://larhyss.net/ojs/index.php/larhyss/index
Received April 3, 2023, Received in revised form June 5, 2023, Accepted June 7, 2023

## ABSTRACT

The experimental study of hydraulic jump characteristics is always a difficult task, particularly regarding the instantaneous velocity, which is difficult to measure experimentally because of its fluctuation and the presence of air bubbles, mainly at the level of the hydraulic jump. However, it is possible to experimentally measure velocities in two-phase flows (air–water) using an intrusive measuring instrument such as a Microreel. This work will experimentally examine two different hydraulic jumps with two flow rates (26.78 l/s and 17.82 l/s) controlled by two thin sills ($H_S$ = 14 cm and $H_S$ = 15 cm) in a channel composed of a trapezoidal shape with a rectangular base. The results of the measurements of the velocities (relative velocity $V^*exp = V/V_0$) as a function of the positions (relative positions $X^* = X/L_s$). The relationship $V^*exp = f(X^*)$ was analyzed by multiple regression and given a second-degree polynomial function. The coefficients of determination of this function are very high ($R^2$ approximately 0.9), which describes a strong relationship between speeds and distances. These results allow us to reflect on the application of learning techniques (ML) to predict relative velocities at any position of the hydraulic jump. Three learning techniques were tested: RBFNN, MPLNN, and GRNN. However, the results prove that the RBFNN has a very accurate speed productivity and records the lowest deviations from the experimental results. Its performance indicators are RMSE = 0.0163 and MAE

= 0.0085 for level 1, RMSE = 0.0138 and MAE = 0.0089 for level 2, and RMSE = 0.0166 and MAE = 0.0099 for level 3. However, the MLPNN model gives competitive results to the RBFNN precisely at level 4, where it registers the smallest deviation (RMSE = 0.0457, MAE = 0.0308).

**Keywords:** Compound Channel, Hydraulic Jump, Machine learning, Relative velocity, Two-phase flow, Velocity Distribution.

## INTRODUCTION

The distribution of velocities in free surface flows (compound bed) is essential for the design and stabilization of hydraulic structures, flood control, and river development projects (Achour and Debabèche, 2003) and (Bousmar et al., 2005). Many experimental investigations have been carried out to clarify the distribution of flow velocities in compound channels, such as the works of (Shiono and Knight, 1991) and (Tominaga and Nezu, 1991), and more particularly, for our area of interest, the work of Chen et al. (2014).

For the passage from a supercritical flow to a subcritical flow in an open channel, the phenomenon of hydraulic jump is the most appropriate, provoking it to occur downstream of hydraulic structures, such as normal weirs, gates and ogee spillways (Saghebian, 2019). The difficulty of studying the hydraulic jump phenomenon in compound channels is due to the implicit interaction between the floodplains (high channel) and the main channel (low channel). This type of flow has yet to be well considered. The few pieces of research that have been conducted are from (Achour and Debabeche, 2003), (Parsaie et al., 2016) and (Benabdesselam et al., 2017). Measuring velocities in the hydraulic jump is one of the most significant difficulties in this field because of their two-phase flows (air–water). (Maatooq and Taleb, 2018) and (Peltier et al., 2013) employed the micropropeller velocimeter in their research work, which is intended for measuring the instantaneous velocities of two-phase flows. Rajaratnam & Subramanya (1968) studied the velocity distribution by measuring the void ratio (air bubble) in the jump (Wang and Chanson, 2015).

The numerical modeling of a hydraulic jump is still a challenging task, owing to its complexity, which involves the rapidly moving free surface, its inherent unsteadiness, which determines the fluctuating position of the roller, strong turbulence effects and the presence of multiphase flow (De Padova et al., 2023). As numerical modeling of the hydraulic jump also still lacks proper validation to accurately calculate air concentration, velocity distribution, and energy dissipation (Carvalho et al., 2008) and (Viti et al., 2018), physical modeling (experimental study) remains the most reliable method for studying the jump (Lubin and Glockner, 2013); (Peltier et al., 2013); (Prosperetti and Tryggvason, 2009). Therefore, the accurate prediction of a numerical model depends on the use of experimental data such as the geometric characteristics and the entry conditions of a flow (the conjugate depths, length of the roll, length of the

jump, mean free surface profile, air concentrations, etc.) (De Padova and Mossa, 2021). Studying flows in compound channels with different experimental configurations is generally associated with artificial intelligence methods. In the same context, we can cite the work of (Mansour-Bahmani et al., 2021) and (Benabdesselam et al., 2022), who deal with the compound channel and modeling via artificial neural network (ANN) methods.

Our work is devised in two parts. The first is physical modeling (experimentation), which consists of carrying out velocity measurements employing a Microreel velocimeter in a hydraulic jump controlled by a thin sill evolving in a channel composed of a trapezoidal shape (major bed) with a rectangular base (minor bed) and zero slope. These measurements are presented in the form of the values of the relative velocities "V*exp" (dimensionless values) on longitudinal profiles according to the relative positions "X*. To demonstrate their correlation, a multiple regression analysis was conducted for the two variables V*=f(X*). The second part is devoted to numerical modeling using machine learning (ML) techniques to predict the relative velocities (V*pred) at any position (X*) in our jump configuration, taking into account their hydraulic and geometric characteristics (Q, V0, H0, HS, LR, LJ, LS) and position (X*, Y) as "input" data of our models. Three models of artificial neural networks have been used: the radial basis function neural network (RBFNN), the multilayer perception neural network (MLPNN), and the generalized regression neural network (GRNN). These three models aim to find the best-predicted velocity values by comparing the performance indices (MAE, RMSE, R2) for the two testing and training phases or by exploiting the experimental velocity results.

## MODELS AND EXPERIMENTAL METHODS

### Physical model

The experimental model (Figs. 1 and 2) consists of a 5 m channel with zero slope, which has a composite shape with a rectangular base (0.2 m*0.2 m) and a trapezoidal cross-section (with a 45° angle of wall inclination). The channel works as a closed circuit being served by a supply basin and draining into another channel of rectangular cross section (0.6 m*0.6 m), in which a rectangular spillway is inserted to allow the direct measurement of the flow. Downstream, a 115 mm diameter pipe in which a pump supplies a box connected to a convergent that flows into the main channel.

The measurement of local (instantaneous) velocity is carried out by a micropropeller velocimeter consisting of a Low-Speed Probe 403 NEXON (range 5-150 cm/sec, accuracy +/- 2% of true velocity) and a digital indicator 430 NEXON, which is connected to a computer to display and record the velocity values. The average velocity is calculated from the downstream measured flow and the surface of the outlet section of the convergent, according to the continuity equation ($V_0 = Q/A_0$).

The average horizontal velocities recorded are measured from a three-dimensional mesh network (XYZ). Along the "y" axis, seven (07) longitudinal sections were distributed over the width of the canal at positions Y (cm) = 0 (central), -4, +4, -8, +8, -10, and +10. Along the "Z" axis, four levels, 10 cm apart between each two successive positions on the "X" axis, were considered.

To properly consider this three-dimensional mesh, we equipped our experimental model with a trolley in the channel, which makes it possible to easily and accurately move the velocimeter probe in the three directions (XYZ). Two rectangular steel sills of different heights (S = 14 cm; S = 15 cm) were designed and included in the channel.

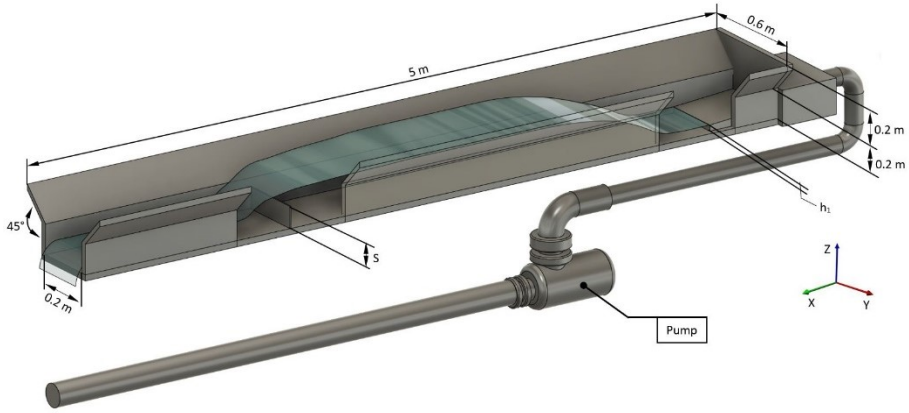


**Figure 1: 3D view of the physical model**

**Figure 2: Photographs showing the physical model and the shape of the canal**

## Artificial neural networks

### *Neural network model description*

The flowchart in Fig. 3 illustrates the process of predicting relative velocities (V*) in a certain position at several planes (Z1, Z2, Z3, Z4) of the flow in the hydraulic jump using three ML models (RBFNN, MLPNN, GRNN) and taking into account input parameters (Q, $V_0$, $H_0$, $H_S$, $L_R$, $L_J$, $L_S$, X*, Y).

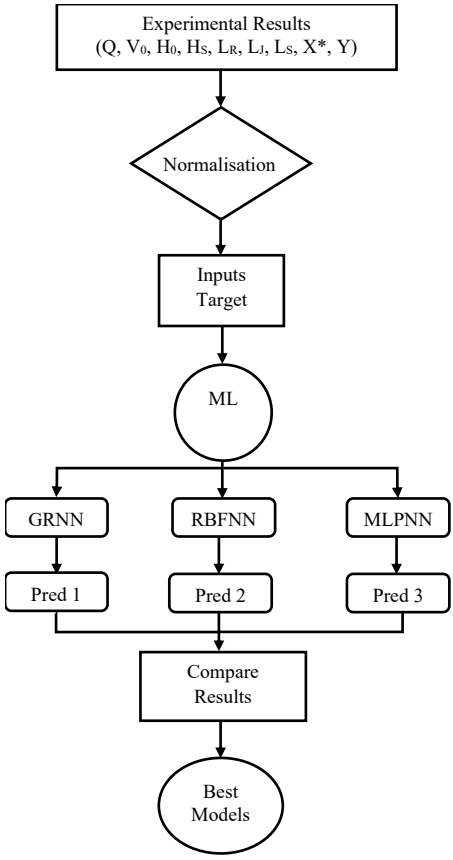


**Figure 3: Flow chart of ML processes for predicting relative velocities (V*)**

#### *Radial Basis Function Neural Network*

In several engineering fields, radial basis function neural networks (RBFNNs) are used for predictive modeling. The RBFNN is illustrated in Fig. 4 as a three-layer architecture. The first layer receives inputs, the second layer is an intermediate layer that includes a

nonlinear RBF activation function, and the third layer makes the prediction (Moody and Darken, 1989); (Haykin, 2009). The following is the RBFNN output equation:

$$y = \sum_{k=1}^{m} \omega_{jk} \theta_k(X) \quad (1)$$

where m is the number of basis functions; X is the input data vector; $\omega_{jk}$ is the weight of the connection between the basis function and output layer; and $\theta_k$ is the nonlinear function of unit 'j', which is usually Gaussian, described by the following expression:

$$\theta_k(X) = exp\left(-\frac{\|X-\mu_k\|^2}{2\sigma_k^2}\right) \quad (2)$$

where X and $\mu$ are the input and center of the RBF unit, respectively. $\sigma_k$ is the spread of the Gaussian basis function.

The weights connecting the hidden neurons to the outputs, centers, and width are regarded as crucial keys in the RBFNN's creation and training.

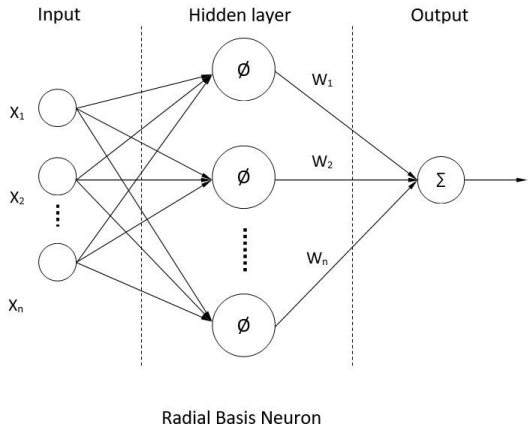


**Figure 4: Structure of a radial basis function neural network (RBFNN).**

***Multilayer Perceptron Neural Network***

The multilayer perceptron model is the most commonly used machine learning approach for feed-forward neural networks. In the hypothesis form $Y = \sum_{i=1}^{n} X_i + b$, the inputs are multiplied by arbitrary weights (wi) and summed by arbitrary bias (b). Then, the hypothesis is nonlinearized using hyperbolic tangent (tansig) as the activation function. In the output layer, a linear function (pureline) was used as the transfer function. Fig. 5 shows a schematic illustration of the multilayer perceptron neural network (MLPNN) architecture. The multilayer perceptron is a type of universal approximator (Haykin, 2009). Using trial and error, the optimal number of perceptrons, hidden layers, and activation functions were obtained.

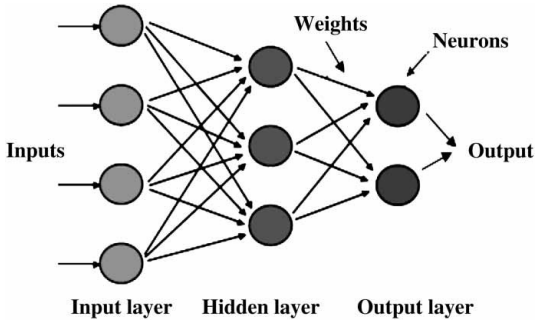


**Figure 5: Schematic representation of the MLPNN model**

***Generalized regression neural network***

The generalized regression neural network (GRNN) is a type of RBNN built on kernel regression. It is an excellent coherent network that may achieve near-zero prediction error with simple function constraints over an extensive training set. Its benefits are tied to consistency. The GRNN architecture is shown in Fig. 6. It does not need an iterative learning process like a back-propagation network.

In GRNN simulations, the problem of local minima does not exist (Specht, 1991). The input vector is stored in a specially built hidden neuron layer. The desired value is assigned to the weights between the output layer and the newly generated hidden layer. The fundamental difference between the two neural networks (GR and RBF) is in the calculation of the values (wij). All the ML models were built in the MATLAB 2019b environment, and the results of this study were carried out using a PC ASUS TUF FX505DT equipped with an AMD Rayzen TM 5 R5-3550H CPU processor at 3.7 GHz and 16 GB of RAM.

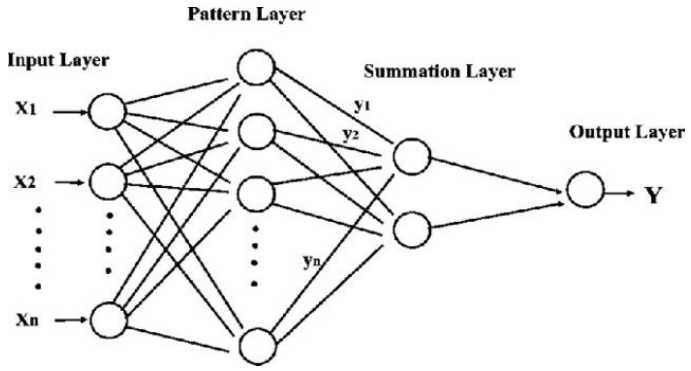


**Figure 6: Structure a generalized regression neural network (GRNN) model.**

### Application of the proposed (ML) models

In the design function approximation of ML models, where we used 70% of the experimental data, one (1) hidden layer is sufficient (Hecht-Nielsen, 1990). Determining the appropriate number of hidden nodes (NHNs) in each layer is one of the core tasks of ML design, and unfortunately, there is no hard and fast rule.

The trial-and-error approach was carried out to find the optimum number of neurons in the hidden layer of the models. The model was determined by varying the number of neurons, starting with a minimum of 3 $(\sqrt{9})$, with N number of inputs and N number of outputs (Masters 1993), then increasing the network size to 19 by adding one neuron each time. It should be noted that 19 is the upper limit for the number of hidden layer neurons needed to map any continuous function work (Hecht-Nielsen, 1990). The training process of the ML model was stopped when the minimum value of MSE for the cross-validation data set was reached.

#### *MLPNN*

The output is the values of the relative velocities (V*pred) of the hydraulic jump in each level Z=1, 2, 3 and 4. On the other hand, as shown above, the inputs are nine parameters (Q, $V_0$, $H_0$, $H_S$, $L_R$, $L_J$, $L_S$, X*, Y). No theory exists of how many hidden units are needed to approximate a given function. The optimal determination of the number of neurons in the hidden layer is the challenge of a test (MATLAB results), which was verified by modifying the number of iterations to reach the best performance values (RMSE and $R^2$). The activation and transfer function used in the study is the hyperbolic tangent (tanh) function.

#### *RBFNN and GRNN*

With the same input–output considerations, both models consist of nine inputs, and concerning the hidden layers, the RBFNN and the GRNN are composed of 90 and 280 neurons, respectively. The spread value proposed for this study was equal to 0.2.

The proposed model is brought to apply a spread that will lead to the most suitable performance with an adaptive value, and it turns out to be unnecessary to modify it in the current study.

## PRESENTATION OF RESULTS

### Experimental results

The experimental results come from two measurement ranges:

- A first series of velocity measurements with 648 points was carried out in the controlled jump caused by a thin sill ($H_S$=15 cm) with a convergent initial height

(H0=3 cm), which gives an initial velocity ($V_0$= 446.26 cm/s). The flow in the canal has a flow rate of Q= 26.78 l/s with a Froude number of F=8.22.

- A second series to confirm the results was carried out at 286 points under entirely different conditions with a second thin sill ($H_S$ = 14 cm) and a new initial height $h_1$ with a new convergent ($H_0$ = 2 cm), which gives a new initial velocity ($V_0$ = 445 cm/s) with a flow (Q = 17.82 l/s) and at a Froude number, F = 10.06.

Due to the very high initial velocities ($V_0$ = 446.26 m/s and 445 m/s) at the exit of the convergent (start of the hydraulic jump), we were unable to measure the velocity over a distance of approximately 110 cm from the convergent for the first range of measurements and 130 cm for the second range.

After the complete formation of the hydraulic jump, we have for each sill height $S_1$ and $S_2$ at their positions $L_{S1}$ and $L_{S2}$ and their initial heights $h_0$ the hydraulic characteristics. These are shown in Tables 1 and 2 for the first and the second series of measurements, respectively.

Relative parameters are calculated from the raw experimental results, such as relative velocity ($V^*exp$) and relative position ($X^*$). This approach aims to find a relationship between the relative velocities and the relative position "$V^* = F(X^*)$". Therefore, the experimental curves were drawn as a function of the values of the relative velocities ($V^*exp$) and the relative positions ($X^*$).

***First series of measurements***

This first series was obtained for a flow rate Q = 26.78 l/s (Table 1), while Fig. 7 shows the variation in the relative mean velocity (V*) as a function of the relative position (X*) for various Y.

**Table 1: Hydraulic characteristics of the controlled hydraulic jump for the first series of measurements**

| $F_r$ | Q (l/s) | $V_0$ cm/s) | $H_0$ (cm) | $H_S$ (cm) | $L_S$ (cm) | $L_R$ (cm) | $L_J$ (cm) |
|---|---|---|---|---|---|---|---|
| 8,22 | 26,78 | 446,26 | 3 | 15 | 400 | 189 | 232 |

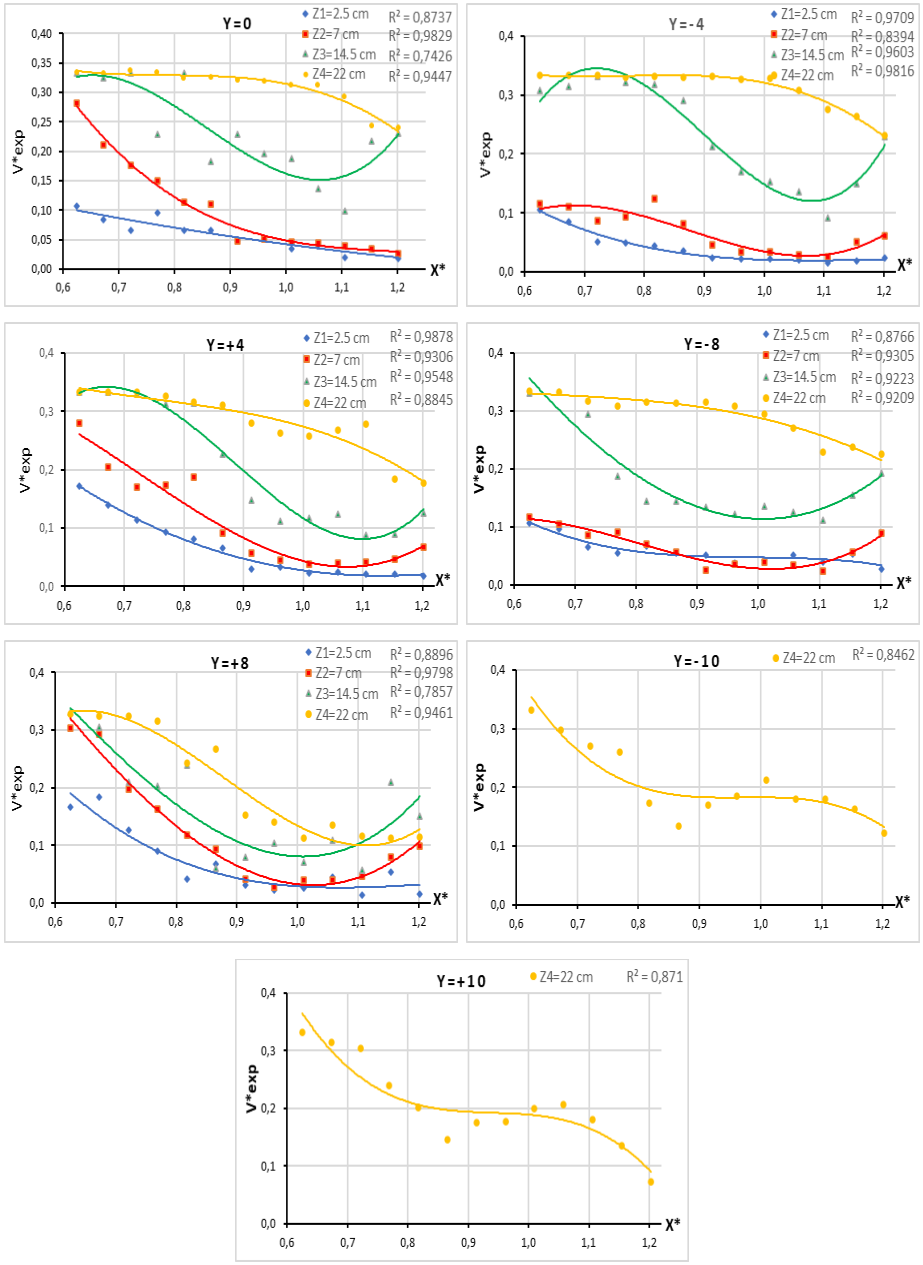


**Figure 7: Variation of relative mean velocity (V*) as a function of the relative position (X*) for Y=0, Y=-4, Y=+4, Y=- 8, Y=+8, Y=-10, Y= +10**

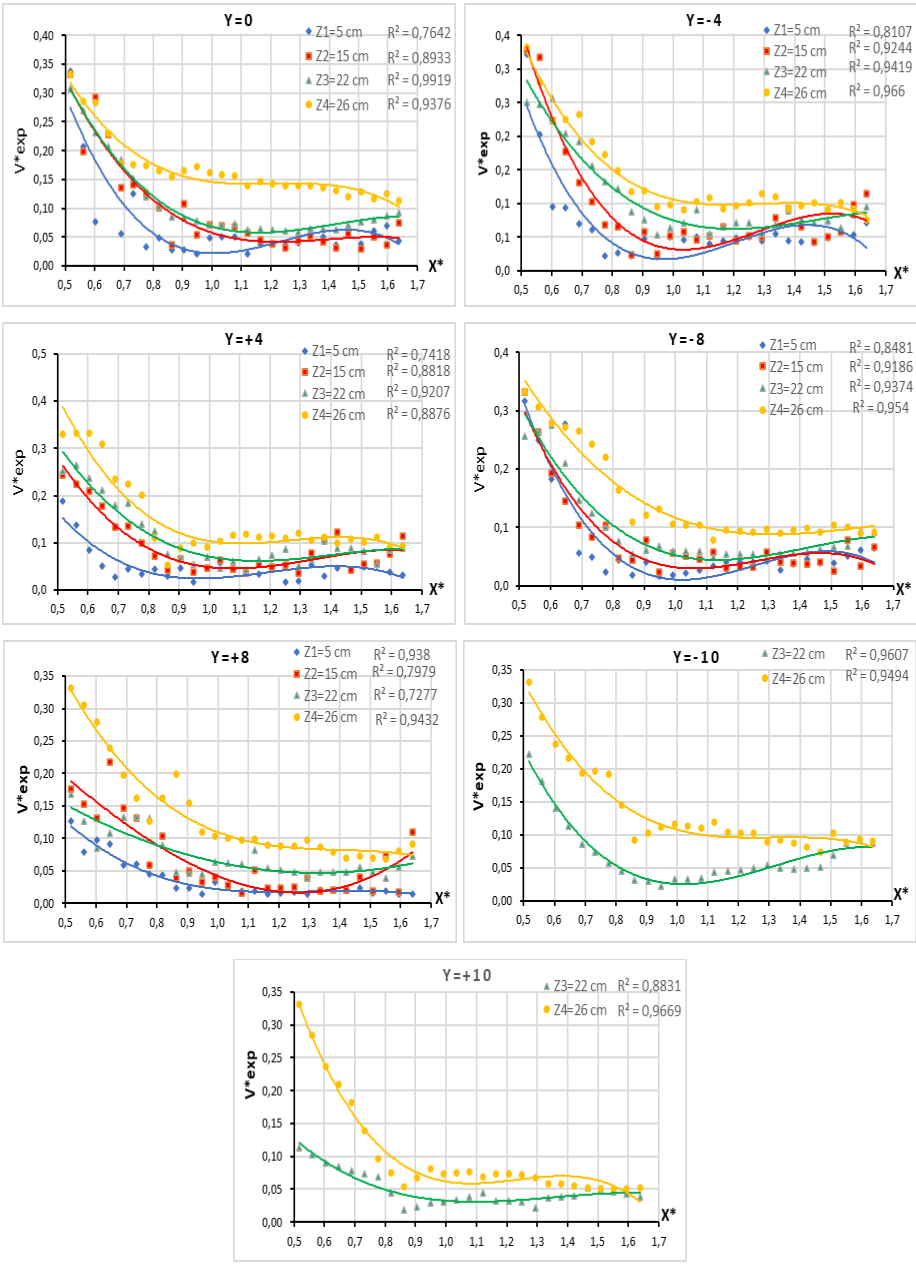


**Figure 8: Variation of relative mean velocity (V*) as a function of the relative position (X*) for Y=0, Y=-4, Y=+4, Y=-8, Y=+8, Y=-10, Y= +10**

**Predictive modeling results**

Taking 70% of the experimental data, models were trained and applied to the other 30% (other positions). Figs. 9, 10 and below illustrates the behavior of the relationship between experimental relative velocities (*V*exp*) and predictive relative velocities (*V*pred*) in four levels of measurement (Z1, Z2, Z3, Z4).

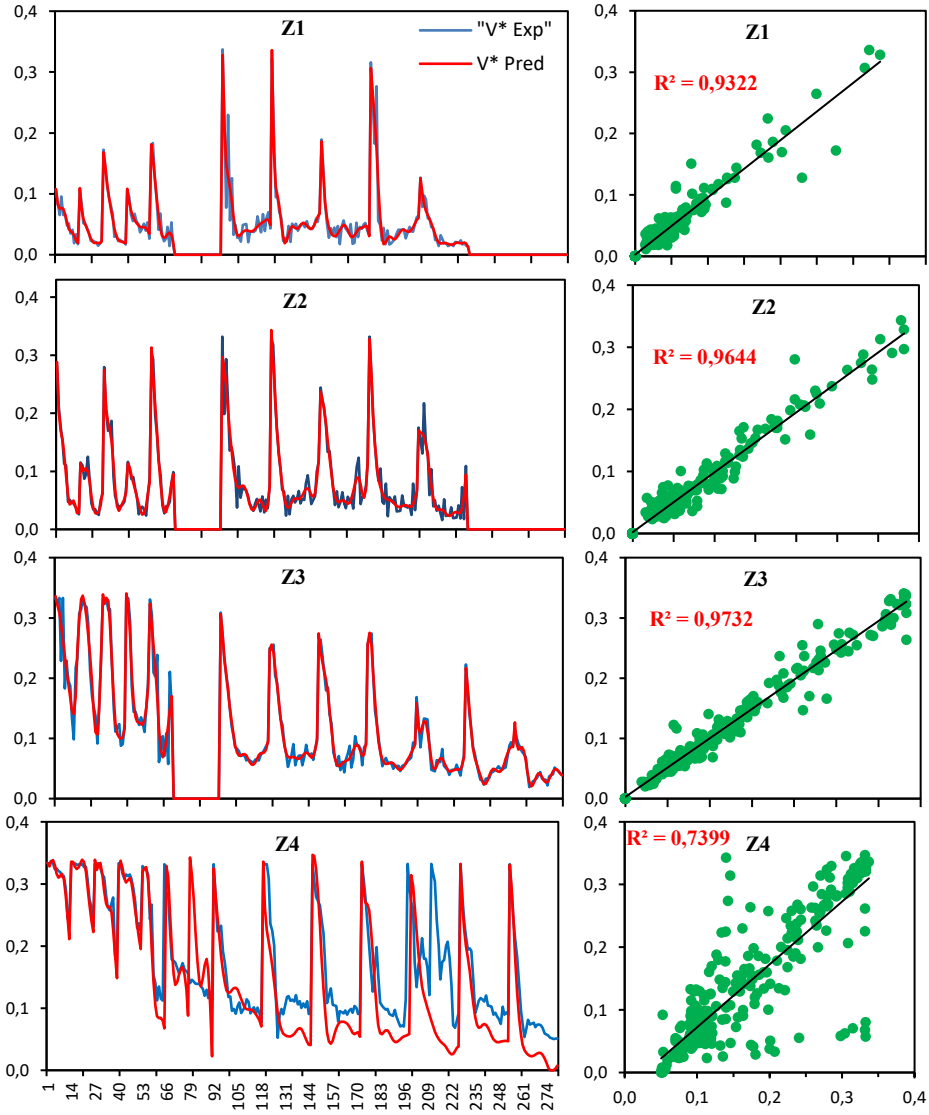


**Figure 9: Performance of the RBFNN model in the test phase for the prediction of relative velocities**

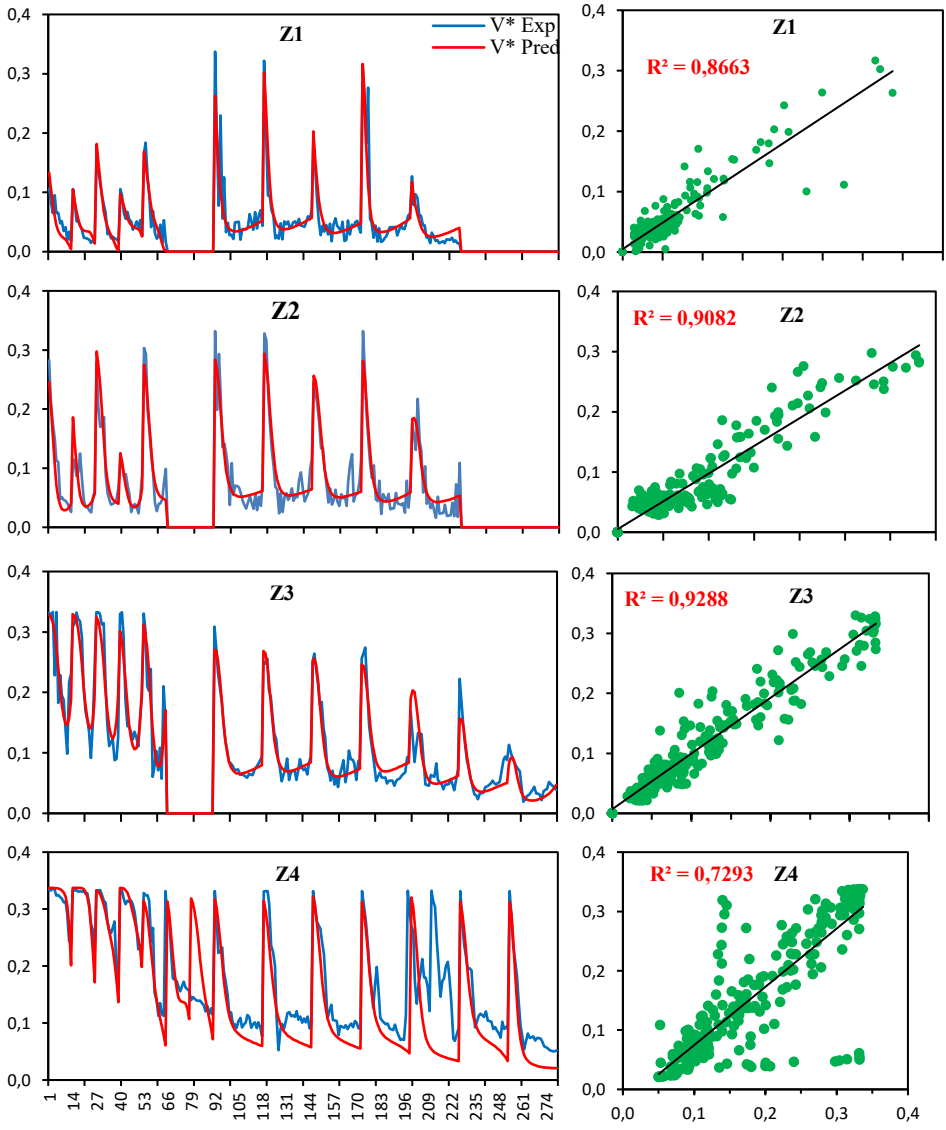


**Figure 10: Performance of the RBFNN model in the test phase for the prediction of relative velocities**

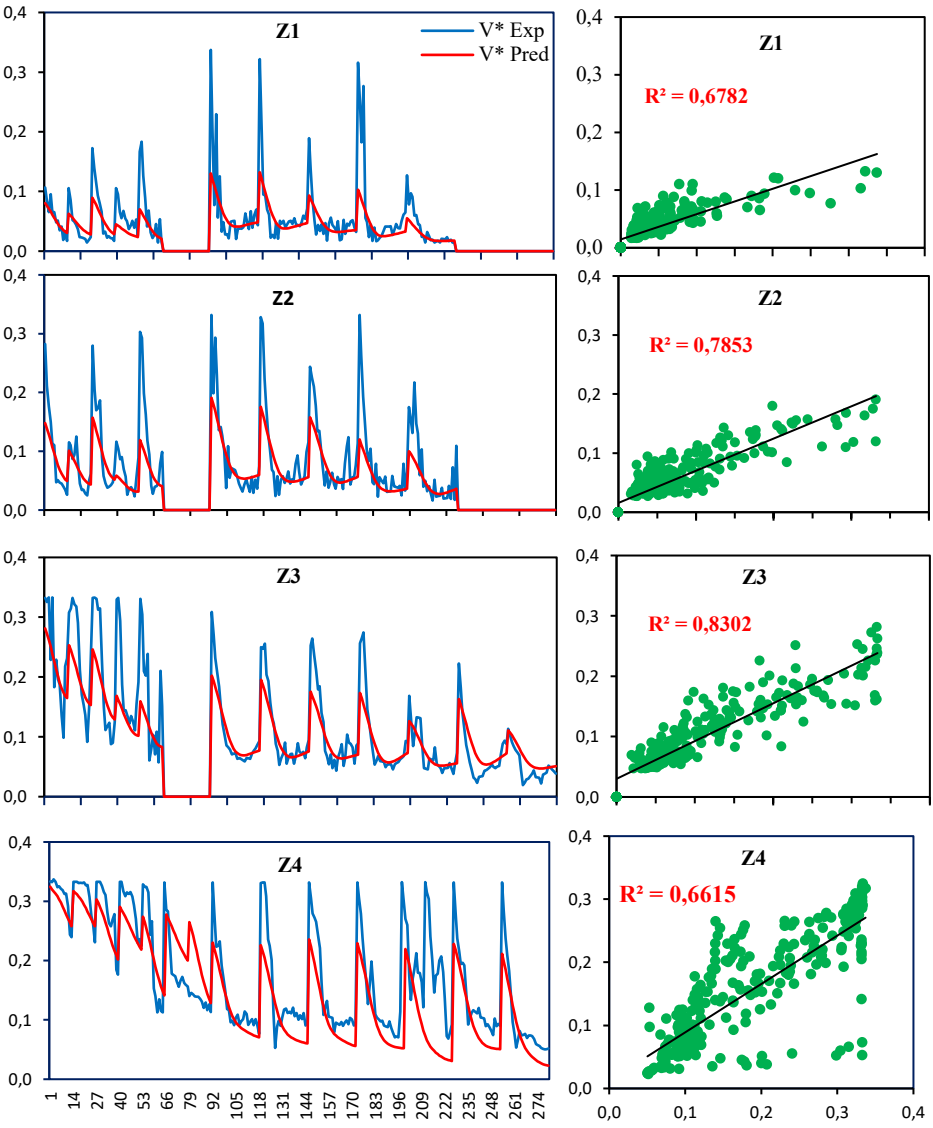


**Figure 11: Performance of the GRNN model in the test phase for the prediction of relative velocities**

## RESULTS AND DISCUSSION

### Discussion of experimental results

The two experiments, being identical in terms of the general distribution of velocities (*V*exp*) as a function of positions (*X**), enabled us to draw the following conclusions:

- At the convergent exit, a high-velocity water jet ($V_0$ approximately 445 cm/s) was generated, causing a flow with very high speeds at the channel bottom (V*exp > 0.33 $V_0$), which cannot be measured until the position X* = 0.5 (Figure 7 and 8). This also occurred in (Chen et al., 2014) experiments. We also noted that for a shallow flow counted from the channel bottom and upstream of the step, the velocities were very high at all points when approaching convergence.
- The high velocities in the upstream part of the hydraulic jump cause a significant flow disturbance (Wang and Chanson, 2015) caused by the high intensity of turbulence occurring near the hydraulic jump's start, which is reduced with distance (Figs. 7 and 8). This turbulence has a significant role in roll generation and creating air bubbles of different sizes. (Chanson, 2009) mentioned in their studies that a hydraulic jump is characterized by large-scale turbulence resulting in the entrainment of air bubbles and a high energy dissipation rate.
- At the end of the hydraulic jump near the sill (approximately X*> 0.84), the velocity at the bottom reaches its minimum value of less than 6 cm/s, while the surface velocity always remains higher in comparison to the bottom (Figs. 7 and 8). As a consequence of this decrease in velocity in the flow, the roll will end with the disappearance of air bubbles, and the water waves decrease; this makes the flow stable (almost uniform), which helps us to determine the final flow height ($H_2$) by continuous observation. At this height, we conclude the approximate length of the jump $L_j$.
- The average velocity, velocity fluctuation and turbulence intensity are all relatively high in the central zone of the flow. Moreover, all these flow parameters decrease toward the lateral walls. These observations are essential for understanding turbulence creation, sediment transport processes, and bank erosion mechanisms; the same conclusion was demonstrated by (Bhowmik et al., 1995). High turbulence levels were recorded in the region of the free surface of the roll. Additionally, some air bubbles in the flow have an opposite direction.
- The equitable distribution of flow between the minor bed (rectangle) and the major bed (trapezium) in our case of the compound channel is made simultaneously with the formation of the roll, and each time the flow increases, a long roll is therefore built (Tables 1 and 2). (Bousmar et al., 2005) noted that a longer distance is needed to balance the flow distribution between the minor bed and major bed subsections.

**Discussion of predictive modeling results**

To achieve the objective of predicting the relative velocities of the hydraulic jump, 12 models were built (an MLPNN model for 4 levels, an RBFNN model for 4 levels and a GRNN model for 4 levels), and their quality was evaluated by means of three parameters: the root mean square error (RMSE), the mean absolute error (MAE) and the coefficient of determination (R). As shown in Table 3, the best model to predict the relative velocity values (*V*pred*) at the 4 levels (Z1, Z2, Z3 and Z4) is the RBFNN with the lowest RMSE and MAE and the highest R values for the test phase. The RBFNN therefore has the best prediction capabilities for the 4 considered levels. The graphic representation is given in Figs. 9, 10 and 11 for the test phases for the 4 levels.

**Table 2: Performance parameters of different ML models.**

| | | TRAIN | | | TEST | | |
|---|---|---|---|---|---|---|---|
| | | RMSE | MAE | R | RMSE | MAE | R |
| **Z1** | **RBFNN** | **0.0163** | **0.0085** | **0.9586** | **0.0044** | **0.0017** | **0.9844** |
| | GRNN | 0.0410 | 0.0212 | 0.7936 | 0.0130 | 0.0048 | 0.9486 |
| | MLPNN | 0.0226 | 0.0128 | 0.9193 | 0.0083 | 0.0043 | 0.9455 |
| **Z2** | **RBFNN** | **0.0138** | **0.0089** | **0.9828** | **0.0129** | **0.0057** | **0.9580** |
| | GRNN | 0.0458 | 0.0271 | 0.8666 | 0.0243 | 0.0099 | 0.9226 |
| | MLPNN | 0.0238 | 0.0169 | 0.9478 | 0.0160 | 0.0082 | 0.9366 |
| **Z3** | **RBFNN** | **0.0166** | **0.0099** | **0.9852** | **0.0069** | **0.0053** | **0.9829** |
| | GRNN | 0.0487 | 0.0312 | 0.9089 | 0.0224 | 0.0173 | 0.8379 |
| | MLPNN | 0.0235 | 0.0159 | 0.9706 | 0.0236 | 0.0149 | 0.8349 |
| **Z4** | **RBFNN** | **0.0457** | **0.0308** | **0.9122** | **0.0882** | **0.0650** | **0.6761** |
| | GRNN | 0.0479 | 0.0388 | 0.8809 | 0.0877 | 0.0616 | 0.5751 |
| | **MLPNN** | **0.0430** | **0.0291** | **0.9207** | **0.0914** | **0.0650** | **0.6174** |

The performance parameters of diverse ML models are displayed in Table 3. These are the results found. First, during the training phase, the RBFNN model showed the lowest errors: RMSE = 0.0163, MAE = 0.0085, for level 1, RMSE = 0.0138, MAE = 0.0089 for level 2, RMSE = 0.0166, MAE = 0.0099, for level 3. However, the level 4 MLPNN model scores the lowest errors (RMSE = 0.0457, MAE = 0.0308). The RBFNN model presents the highest accuracy (R = 0.9586) for level 1, R = 0.9828 and R = 0.9852 for level 2 and level 3, respectively. In level 4, the MLPNN model (RMSE = 0.0430, MAE= 0.0291, R = 0.9207) remains the best model.

During the testing phase, the RBFNN model proves strong robustness in the prediction task with the lowest errors RMSE= 0.0044, MAE= 0.0017, RMSE= 0.0129, MAE= 0.0057, RMSE= 0.0069, MAE= 0.0053, RMSE= 0.0882, MAE= 0.0650 in levels 1, 2, 3, and 4, respectively. In level 4, one more RBFNN model demonstrates better modeling capacities with the highest accuracy (R = 0.6761).

The Taylor diagram was used as a basic tool to illustrate the prediction model characteristics (Taylor, 2001). Because of the benefits of integrating and assessing various statistical performance indicators, it is the most general proposed diagram for comparing accuracy. It was also employed as a simple tool to represent the details of the predictive models in this study. When the predicted values are closer to the experimental values, this indicates that the proposed model has excellent generalization capabilities, which are manifested by a standard deviation (SD) value very close to the observed value (SD), higher R, close to 1, and root mean square deviation (RMSD) minimal and close to 0.

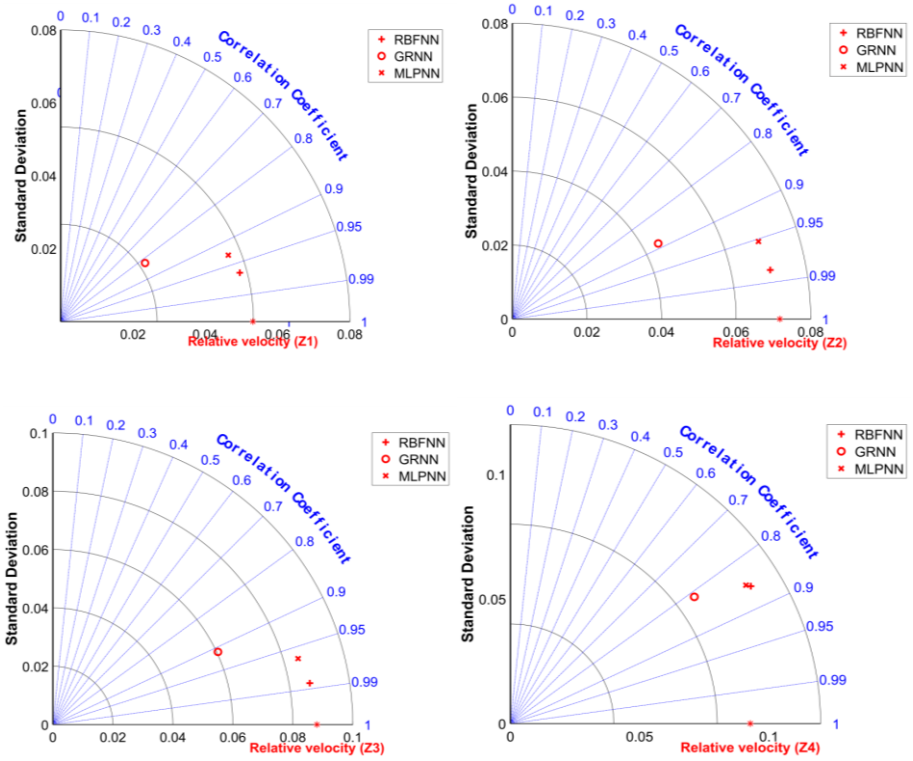


**Figure 12: Taylor diagram showing the performance of ML models applied for different levels.**

Fig. 12 illustrates the efficiency of the RBFNN model in predicting relative velocity. The correlation decreases if a value goes to higher zones in the diagram. The RMSD shows the quality of the ML model. Based on Table 4, the SD of the predicted values generated by the RBFNN models is closer to the SD of the experimental data for the four levels. High R = 0.9654, 0.9818, 0.9864, and 0.8597 for levels 1, 2, 3 and 4,

respectively, show a high level of harmony between the experimental and predicted values.

**Table 3: Statistics parameters (SD, RMSD) of different ML models.**

| | RMSD | | | | SD | | | |
|---|---|---|---|---|---|---|---|---|
| | Z1 | Z2 | Z3 | Z4 | Z1 | Z2 | Z3 | Z4 |
| **Exp. Data** | 0 | 0 | 0 | 0 | 0.0532 | 0.0717 | 0.0881 | 0.0928 |
| **RBFNN** | 0.0139 | 0.0135 | 0.0144 | 0.0551 | 0.0513 | 0.0704 | 0.0868 | 0.1081 |
| **GRNN** | 0.0339 | 0.0385 | 0.0414 | 0.0553 | 0.0284 | 0.0441 | 0.0604 | 0.0875 |
| **MLPNN** | 0.0195 | 0.0218 | 0.0235 | 0.0556 | 0.0498 | 0.0693 | 0.0849 | 0.1068 |

To confirm the robustness of the proposed model, the analysis of the RMSD values of the different models applied to levels 1, 2, 3 and 4 shows that the RMSD values of the RBFNN model are very close to 0.

## CONCLUSION

In this work, a physical model of a compound channel was used to form two different hydraulic jumps and allow point velocity measures in the hydraulic jumps, which were used to construct machine learning models and predict velocities in other locations. The models were compared to each other and with the remaining experimental data. We employed three models of machine learning techniques to predict relative velocities in the hydraulic jumps. The comparison of the different models (RBFNN, MLPNN and GRNN), taking into account all the characteristics of the hydraulic jump and the location point (Q, $V_0$, $H_0$, $H_S$, $L_R$, $L_J$, $L_S$, X*, Y), shows that RBFNN gives the best results for “TEST » and « TRAIN » compared to the other two models. Thus, RBFNN can predict relative velocity ratios with high accuracy compared to other models. At the same time, MLPNN remains a competitive model with RBFNN, especially in the channel bottom velocity (level 4), where there is high flow turbulence.

The recommended ML models (RBFNN and MLPNN) in this study have shown that they can capture the processes of the hydraulic jump phenomenon from the input information and predict velocity results very similar to the experimental data. We can then consider the high predictive potential of the models as a tool for modeling, as from part of the experimental data (inputs), they can easily and quickly predict the velocity in other locations of hydraulic jumps with great accuracy.

It is worth mentioning that the present models can work and give the four-level velocities (Z1, Z2, Z3, Z4) of the hydraulic jump in a compound channel. These models are confined to an interval of flow rate (Q= 17,82 l/s and Q= 26,78 l/s), as shown above.

These results motivate us to work on the realization of the models with a considerable interval in terms of flow rate so that they have wide use in the field.

The variation in the relative velocities ($V^*exp$) along the relative positions ($X^*$) is translated by a second-degree polynomial function for all the longitudinal sections "Y", with very high coefficients of determination (an average of $R^2 \approx 0{,}9$).

**Declaration of competing interest**

The authors declare that they have no known competing financial interests or personal relationships that could have appeared to influence the work reported in this paper.

**REFERENCES**

ACHOUR B., DEBABÈCHE M. (2003). Ressaut contrôlé par seuil dans un canal profilé en U, Journal of Hydraulic Research, Vol. 41, No 1, pp. 97-103. (In French)

ACHOUR B., DEBABÈCHE M. (2003). Control of hydraulic jump by sill in triangular channel, Journal of Hydraulic Research, Vol. 41, No 3, pp. 319-325. (In French)

BENABDESSELAM A., ACHOUR B., HOUICHI L. (2017). Hydraulic jumps in a straight rectangular compound channel: Theoretical approach and experimental study, Larhyss Journal, No 29, pp. 323-340.

BENABDESSELAM A., HOUICHI L., ACHOUR B. (2022). GRNN-based models for hydraulic jumps in a straight rectangular compound channel, Modeling Earth Systems and Environment, Vol. 8, pp. 1787-1798.

BHOWMIK N.G., MAZUMDER B.S., XIA R., SOONG T.W. (1995). Distribution of turbulent velocity fluctuations in a natural river, Journal of Hydraulic Research, Vol. 33, pp. 649-661.

BOUSMAR D., RIVIERE N., PROUST S., PAQUIER A., MOREL R., ZECH Y. (2005). Upstream discharge distribution in compound-channel flumes, Journal of Hydraulic Engineering, Vol. 131, pp. 408-412.

CARVALHO R., LEMOS C., RAMOS C. (2008). Numerical computation of the flow in hydraulic jump stilling basins, Journal of Hydraulic Research, Vol. 46, No 6, pp. 739-752.

CHANSON H. (2009). Current knowledge in hydraulic jumps and related phenomena. A survey of experimental results, European Journal of Mechanics - B/Fluids, Vol. 28, Issue 2, pp. 191-210.

CHEN J., ZHANG J., XU W., PENG Y. (2014). Characteristics of the velocity distribution in a hydraulic jump stilling basin with five parallel offset jets in a twin-layer configuration, Journal of Hydraulic Engineering, Vol. 140, pp. 208-217.

DE PADOVA D., MOSSA M. (2021). Hydraulic jump: a brief history and research challenges, Water, Vol.13, Paper 1733.

DE PADOVA D., MOSSA M., SIBILLA S. (2023). SPH modelling of hydraulic jump at high Froude numbers at an abrupt drop: vorticity and turbulent pressure fluctuations, Environmental Fluid Mechanics, Vol. 23, pp. 511-531.

HAYKIN S. (2009). Neural networks and learning machines, 3rd Ed., Pearson Education, India.

HECHT-NIELSEN R. (1990). On the algebraic structure of feedforward network weight spaces, Advanced Neural Computers, Elsevier, pp. 129-135.

LUBIN P., GLOCKNER S. (2013). Detailed numerical investigation of the three-dimensional flow structures under breaking waves, Proceedings 7th International Conference on Coastal Dynamics Conference, pp. 1127-1136.

MAATOOQ J., TALEB E. (2018). The effects of baffle blocks locations and blockage ratio on the sequent depth and velocity distribution of forced hydraulic jump, International Symposium on Hydraulic Structures, Utah State University, USA.

MANSOUR-BAHMANI A., HAGHIABI A.H., SHAMSI Z., PARSAIE A. (2021). Predictive modeling the discharge of urban wastewater using artificial intelligent models (case study: Kerman city), Modeling Earth Systems and Environment, Vol. 7, pp. 1917-1925.

MOODY J., DARKEN C.J. (1989). Fast learning in networks of locally tuned processing units, Neural computation, Vol. 1, pp. 281-294.

PARSAIE A., HAGHIABI A.H., SANEIE M., TORABI H. (2016). Prediction of energy dissipation on the stepped spillway using the multivariate adaptive regression splines, ISH Journal of Hydraulic Engineering, Vol. 22, Issue 3, pp. 281-292.

PELTIER Y., PROUST S., RIVIERE N., PAQUIER A., SHIONO K. (2013). Turbulent flows in straight compound open-channel with a transverse embankment on the floodplain, Journal of Hydraulic Research, Vol. 51, Issue 4, pp. 446-458.

PROSPERETTI A., TRYGGVASON G. (2009). Computational methods for multiphase flow, Cambridge university press.

SAGHEBIAN S.M. (2019). Predicting the relative energy dissipation of hydraulic jump in rough and smooth bed compound channels using SVM, Water Supply, Vol. 19, Issue 4, pp. 1110-1119.

SHIONO K., KNIGHT D.W. (1991). Turbulent open-channel flows with variable depth across the channel, Journal of fluid mechanics, Vol. 222, pp. 617-646.

SPECHT D.F. (1991). A general regression neural network, IEEE transactions on neural networks, Vol. 2, pp. 568-576.

TAYLOR K.E. (2001). Summarizing multiple aspects of model performance in a single diagram, Journal of Geophysical Research: Atmospheres, Vol. 106, pp. 7183-7192.

TOMINAGA A., NEZU I. (1991). Turbulent structure in compound open-channel flows, Journal of Hydraulic Engineering, Vol. 117, pp. 21-41.

VITI N., VALERO D., GUALTIERI C. (2018). Numerical simulation of hydraulic jumps, Part 2: Recent results and future outlook, Water, Vol. 11, Issue 1, Article 28.

WANG H., CHANSON H. (2015). Experimental study of turbulent fluctuations in hydraulic jumps, Journal of Hydraulic Engineering, Vol. 141, Paper 04015010.